

# Predicting *Sphaeropsis sapinea* Damage in *Pinus radiata* Canopies Using Spectral Indices and Spectral Mixture Analysis

Nicholas C. Coops, Nicholas Goodwin, and Christine Stone

## Abstract

Maintaining the health and condition of the forest plantation estate is critical to ensuring there are no adverse losses in productivity. Within Australian *Pinus radiata* plantations a diverse range of damaging agents are present. One significant agent is a fungal pathogen *Sphaeropsis sapinea*. In this research, we detail the development of relationships between a range of individual crown health attributes representing symptoms of *Sphaeropsis sapinea* infection and high spatial and spectral resolution remotely sensed imagery characteristics. To do this, two methods were used; the first utilized vegetation spectral indices including simple and normalized difference ratios, and the second, linear spectral mixture analysis. Results indicate that spectral indices that utilize either chlorophyll absorption wavelengths at 680 nm with a non-chlorophyll region of the spectrum (such as 710 or 750 nm) or the slope of the upper red-edge between 710 and 740 nm were most significantly related to individual crown damage attributes. Linear unmixing analysis consistently extracted four fraction endmember images (sunlit canopy, soil, shadow, and non-photosynthetic vegetation (NPV)) from the 12 channel imagery. Multiple linear stepwise regression models developed using mixed fractional abundances provided similar results to those derived using spectral indices. The NPV and shadow endmembers, in order, were consistently identified as the most significant in these developed models.

## Introduction

Australian softwood, *Pinus radiata* (D. Don), plantations contain a number of abiotic and biotic damaging agents that affect the health of the forest (Will, 1985; Bollmann *et al.*, 1986; Lewis and Ferguson, 1993). *Sphaeropsis sapinea* (formerly known as *Diplodia pinea*) is one of the most severe and ubiquitous. Under weather conditions favorable for infection (wet and warm weather), the fungus penetrates

succulent stems through the intact epidermis and enters needles through stomata. The fungus may also infect stems and older branches through fresh wounds inflicted by insects, hail, or damaging agents. This capacity to infect a range of host tissue types can result in a number of different symptoms including needle discoloration, shoot blight or die-back, stem cankers, root diseases, and blue stain. Many of these symptoms become apparent after hail damage or when the tree is stressed due to environmental factors such as drought. While tree death rarely occurs, severe malformation resulting from repeated attacks has been shown to have a major effect on potential stand volume.

Improvements in remote sensing technologies, particularly in the spatial and spectral resolution of optical sensors, have made the prospect of using digital remotely sensed imagery to detect and classify stressed vegetation a realistic and attractive option (Franklin, 2000). A number of different approaches have been used to derive forest health and condition from remote sensing imagery. These include the use of narrow band spectral indices which are sensitive to leaf pigment content (Datt, 1998; Zarco-Tejada *et al.*, 2002) and crown biomass (Spanner *et al.*, 1990a and 1990b; Coops *et al.*, 2002) and the use of image fractions derived from endmembers which represent the spectral characteristics of cover types regarded as having uniform properties (Garcia-Haro *et al.*, 1999). The use of narrow-band spectral indices is the most widely applied, however, a potential limitation with the use of spectral indices is that they are often calculated from a small number of spectral bands, usually two, and thus do not utilize new and potentially important information in other channels (Peddle *et al.*, 2001).

In addition to using spectral image information to assess canopy condition, research has also demonstrated that structural change occurs at both an individual crown or forest canopy scale (e.g., Wulder *et al.*, 2004). High spatial resolution imagery, with pixels smaller than the dimensions of individual tree crowns, allows the derivation of variance measures and spatial statistics which have been related to the physical structure of individual trees. For example, the relationship between shadow in a patchy canopy compared to a bright full and dense canopy (e.g., Gougeon, 1999; Lévesque and King, 1999; Olthof and King, 2000) has been modeled using high spatial resolution imagery.

---

N.C. Coops was formerly at CSIRO Forestry and Forest Products, Private Bag 10, Clayton South 3169, Victoria, Australia, and is now at the Department of Forest Resource Management, 2424 Main Mall, University of British Columbia, Vancouver, Canada (Nicholas.coops@ubc.ca).

Nicholas Goodwin is at CSIRO Forestry and Forest Products, Private Bag 10, Clayton South 3169, Victoria, Australia, University of New South Wales.

Christine Stone is with the Research and Development Division, State Forests on NSW, P.O. Box 100, Beecroft, NSW 2119.

---

Photogrammetric Engineering & Remote Sensing  
Vol. 72, No. 4, April 2006, pp. 405–416.

0099-1112/06/7204-0405/\$3.00/0  
© 2006 American Society for Photogrammetry  
and Remote Sensing

In this paper, we compare the capability of CASI-2 high spectral and spatial resolution imagery to detect the occurrence and severity of *Sphaeropsis sapinea* outbreaks in *Pinus radiata* crowns using two general techniques: narrow-band spectral indices and image fractions derived from endmembers. The work is undertaken within *P. radiata* plantations in New South Wales (NSW) which are subject to outbreaks of *Sphaeropsis sapinea*. The overall aim is to develop a generic, operational crown based index, suitable for use in *P. radiata* stands throughout NSW and Australia.

## Study Area and Datasets

### Description of Study Site

The study site was located in the Kangaroo Vale Section of Buccleuch State Forest, in southern NSW (35°06'S, 148°17'E; 450 m Elevation), Australia. The site is classified as a metabasic igneous complex with relatively shallow soils. It has a winter dominated rainfall and often hot dry summers resulting in the area being prone to drought. Ground-based assessment plots were established in two adjacent *P. radiata* compartments planted in 1992 on flat terrain. Neither had been thinned, but manual pruning of selected trees had been applied. The compartments in Kangaroo Vale Section have a history of tree death from *S. sapinea* and, at the time of the ground-based assessments and image acquisition, they presented trees exhibiting a range of symptoms.

### Acquisition of Imagery

Imagery was collected from the Compact Airborne Spectrographic Imager 2 (CASI-2). CASI-2 is an airborne push-broom spectrographic imager that acquires imagery in the visible and near-infrared regions of the electromagnetic spectrum between 413 nm and 958 nm (Shepherd *et al.*, 1995; Treitz and Howarth, 1996). To minimize bidirectional reflectance and to cover the study area, flight lines were oriented parallel to the solar azimuth (i.e., away from the sun). Imagery was flown at an altitude of 3,300 m as a single strip on 03 September 2002 under clear sky conditions with maximum solar elevation angle with a swath width of 400 m. September was chosen as it is just prior to the emergence of new shoot growth when mature foliage would have approximately one year's cumulative damage. Flight lines covered two pseudo invariant features (PIFS) (large sheets of uniform reflectance fabric material, one black, the other white) which were positioned by field personal to assist in image calibration. Spectral reflectance measurements of the PIFS were acquired at the same time of image overpass using a Uni-Spec Spectrometer which measures radiation from 350 to 1100 nm. The imagery was collected at a spatial ground resolution of 0.8 m in 12 spectral bands (Table 1) which

were pre-selected after an independent examination of needle-based spectra of healthy and damaged needles to provide maximum spectral discrimination (Stone *et al.*, 2003). An empirical line correction routine (Farrand *et al.*, 1993) was used to relate the PIF reflectance's measured at time of overpass to the CASI-2 digital numbers resulting in a function which transformed the entire image to reflectance units. While temporal analysis was not undertaken as part of this study, basic atmospheric correction and conversion to reflectance was essential for the spectral unmixing algorithm (described later) and comparison of the magnitude and range of index values with other studies.

### Ground-based Assessment

Field data collection followed one week after image capture, as it was essential to ensure individual tree crowns were correctly identified and assessed in the field and matched to the respective crowns in the imagery. Previous work has demonstrated that when field programs have been undertaken without access to the high spatial resolution imagery, matching tree crowns on the imagery has proven to be difficult (Coops *et al.*, 2002) and, as a result, it was assumed there was no change in canopy condition over the intervening one week period. The field team consisted of forest health experts with significant experience in detecting and assessing forest health both in Australia and overseas. Three plots were located within the study site. Two plots (6 × 4 rows of trees, 24 trees total) and the third (6 × 5 rows of trees, 30 trees total) were placed to ensure they contained crowns exhibiting a range of symptoms. Each individual tree crown was then measured and/or assessed by the field team.

A key initial indicator in the presence and identification of *S. sapinea* is the presence of orange needles along the leader or outer branch, resulting in dead tops, followed by an increasing number of dying branches. As the lower crown can remain dark green with normal foliage density, estimates of crown color in horizontal quartiles with a comparison of the lower to upper crown can provide an indication of *S. sapinea* severity. The color within each quartile is therefore assumed to be constant. At the needle scale, the visual symptoms include needles becoming uniformly paler green, wilting (briefly), then turning yellow through orange and red, and ultimately being shed. A nominal color code was established with healthy (dark green crowns equal to 1, 2: light green, 3: yellow, 4: orange, 5: red, and 6: grey). In order to assess the crown color, two forest health experts worked as a team. First, a number of key crowns, of varying color, were individually assessed and compared to ensure consistent color scoring. Once both members observed the same color scores, each crown was then scored individually and scores compared between observers. If observer's scores differed, the crowns were reassessed from different viewing angles. Any final adjudication was left to the senior forest health expert. After two trial plots, both observers color scores agreed in over 90 percent of the observations indicating high precision of the visual estimates. A mean crown color score was also computed as the average of the upper crown components multiplied by the color of the leader (scaled between 0 and 1). High mean crown color scores are indicative of crowns which have needle color associated with severe damage and lower scores are associated with trees that have no color variation and are all dark green (between 0 and 1). Table 2 details the measured field attributes for the stands.

During the field campaign, reflectance measurements were made of a number of key cover types including a series of dry soil samples from roads and cuttings, healthy and unhealthy foliage, and dead non-photosynthetic material such as bark and dead needles. Each sample was either

TABLE 1. CASI-2 SPECTRAL WAVELENGTHS

Band Number	Band Location (nm)	Bandwidth
1	450	13
2	550	12
3	635	12
4	679	12
5	690	12
6	701	10
7	710	10
8	720	10
9	730	10
10	740	12
11	751	10
12	850	12

TABLE 2. ANALYZED FIELD ATTRIBUTE INFORMATION COLLECTED FOR TREE CROWNS WITH *S. SAPINEA* INFECTION

	Tree Height (m)	DBH (cm)	Leader Color	Top 1/4 Color	Presence of Dead Leader (*)	Presence of Discoloration (*)	Mean Crown Condition
N (samples)	78	78	78	78	78	78	78
Mean	26.2	36.1	2.1	1.96			0.2
Minimum	17.7	22.2	1	1	Y	Y	0.03
Maximum	42.0	53.1	6	6	N	N	1
Std. Dev.	4.1	6.7	1.9	1.76			0.3

Note: 1: Dark Green, 2: Light green; 3: Yellow; 4: Orange; 5: Red; 6: Grey.  
 (\*): Categorical Variable (Y: Yes, N: No).

stacked (in the case of foliage) or layered (in the case of soil) to cover an area of approximately 10 cm × 10 cm. The UniSpec Spectrometer was used to measure needle reflectance. Five reflectance measurements were averaged to obtain a mean reflectance spectrum using a 150 W halogen bulb to illuminate the leaves. A calibrated panel of known reflectance was used as a “white” reference and was measured prior to each set of spectral readings. Target reflectance was calculated as the ratio of energy reflected from the target to energy incident on the target.

When utilizing high spatial resolution imagery, such as the 0.8 m CASI-2 reflectances, the method used to generate the spectral response for each individual crown is an important issue. When viewing high spatial resolution imagery of tree crowns, significant brightness variation exists depending on the pixel position within the crown. This effect is caused by a number of factors including differences in illumination due to canopy and leaf geometry, the viewing angle, and the bidirectional reflectance distribution function (Li and Strahler, 1985). In a study of these effects on individual crown delineation Leckie *et al.*, (1992) compared a number of sampling methods to extract the spectral characteristics of individual tree crowns. These included the average of pixel brightness for the whole tree; the sunlit portion, the shaded portion or the maximum brightness from a single pixel at the top of the tree (Leckie *et al.*, 1992). It was concluded that either the whole tree or the sunlit tree sampling methods were the most suitable methods to derive consistent and representative spectral response for crown modeling (Leckie *et al.*, 1992). Based on this result whole crown boundaries were located on large scale hardcopies of the imagery and the boundaries manually digitized.

## Methods

### Modeling Methodology

In this paper we compare the capability of CASI-2 high spectral and spatial resolution imagery to detect the extent and severity of *Sphaeropsis sapinea* outbreaks on *Pinus radiata* crowns using two broad techniques: narrow band spectral indices and the use of image fractions derived from endmembers.

### Spectral Indices

A number of reviews provide a synthesis of indices that have been applied to vegetation spectra (e.g., Carter and Miller, 1994; Merton, 1999; Thenkabail *et al.*, 2000; Sims and Gamon, 2002). These indices often either target the leaf pigment content, such as chlorophyll (Carter and Knapp, 2001; Gitelson *et al.*, 2003 and references therein) or leaf water content (Peñuelas *et al.*, 1997; Datt 1999). Generally, the reflectance indices can be grouped into three broad types: simple ratios, normalized differences, and red edge indices (Sims and Gamon, 2002). Historically, simple and normalized

difference reflectance indices were developed as vegetation abundance indices and compared reflectance at key absorption wavelengths, the most common of which is the simple vegetation index. Recently, using narrow band spectral wavelengths, they have been applied as vegetation stress indicators (Sims and Gamon, 2002). Red-edge based indices compare the spectral region between 690 to 750 nm which is sensitive to strong absorption by chlorophyll in the red region and strong reflectance in the NIR region due to scattering in the leaf mesophyll and the absence of absorption by pigments (Gausman, 1985). With 12 spectral channels available on the CASI-2, only a selected subset of previously published indices were able to be calculated. The indices applied in this study include standard measures of the red-edge, in particular the total, mean, maximum, median, upper and lower slope, and the inflection point of the red-edge. The ratio-based indices used include a range of standard vegetation normalized ratios including the NDVI and SAVI and some specific plant stress based indices, the Carter (1994) plant stress index, two chlorophyll ratios using the blue (Peñuelas *et al.*, 1995), and NIR (Gitelson *et al.*, 2003) regions, Stone *et al.* (2003), the Plant Senescence Reflectance Index (PSRI) (Merzlyak *et al.*, 1999), and two recent indices from Sims and Gamon (2002) which are modified simple and normalized ratios that use the reflectance at 450 nm as a stable wavelength.

Table 3 lists the spectral indices, transferable to the CASI-2 sensor which were used in this study.

### Linear Spectral Unmixing Analysis

Linear spectral unmixing modeling assumes that each pixel's value is a linear combination of reflectance from a limited set of constituent elements, called endmembers (Ustin *et al.*, 1995). For a given wavelength channel ( $i$ ), the constrained pixel reflectance ( $R_i$ ) of a given pixel can be expressed using Equation 1 and constrained by Equation 2:

$$R_i = \sum_{j=1}^n f_j RE_{ij} + \varepsilon_i \quad (1)$$

$$0 \leq \sum_{j=1}^n f_j \leq 1 \quad (2)$$

where  $f_j$  is the endmember image fraction,  $RE_{ij}$  is the reflectance of image endmember,  $j$ , at band  $i$ ,  $n$  is the number of endmembers, and  $\varepsilon_i$  is the residual error for band  $i$  (van de Meer and de Jong, 2000). If the number of wavelength channels is at least as large as the number of endmembers, then endmember spectral values observed in the field or using image interpretation, can be used to obtain estimates of the fraction of each pixel that is in each endmember.

The method assumes that the reflectance from each pixel is a linear combination of each endmember and the fractional abundances are computed on a pixel by pixel basis (Okin and Roberts, 2000). The assumption of linearity

TABLE 3. SPECTRAL INDICES USED TO ASSESS CROWN CONDITION

Reflectance Index	Formulation	Reference
Slope of Red-Edge	R740-R690/N <sub>740-690</sub>	Merton (1999)
Slope of Lower RE	R710-R690/N <sub>710-690</sub>	Merton (1999)
Slope of Upper RE	R740-R710/N <sub>740-710</sub>	Merton (1999)
Mean Slope of RE	(R690 to R740)/N	Merton (1999)
Max Slope of RE	Max [(R690 to R740)/N]	Merton (1999)
Median Slope of RE	Median [(R690 to R740)/N]	Merton (1999)
Stone Needle Damage	R709/R691	Stone (2003)
Peñuelas	R430/R680	Peñuelas (1995)
Carter (C1)	R690/R750	Carter (1994)
Carter (C3)	R710/R760	Carter (1994)
Red-Green Index	R740/R550	Huete (1988)
Total Chlorophyll	R750/R550	Gitelson and Merzlyak (1996)
NDVI	(R750 - R550)/ (R750 + R550)	Huete (1988)
SAVI	1.5 * ((R750 - R550)/ (R750 + R550 + 0.5))	Huete (1988)
mSR <sub>index</sub>	(R750 - R450)/ (R700 + R450)	Sims and Gamon (2002)
mND <sub>index</sub>	(R750 - R680)/ (R750 + R680 - 2*R450)	Sims and Gamon (2002)
Plant Senescence Reflectance Index (PSRI)	(R680 - R500)/ R750 Note: R500 replaced with R450	Merzlyak <i>et al.</i> , (1999)

Note: R = reflectance at given wavelength, N = wavelength difference in nm between reflectance spectra.

is arguably the most important problem with linear mixture modeling (Roberts *et al.*, 1993). Non-linear mixing can be expected in vegetation canopies as green vegetation transmission is high at certain wavelengths, however in the short-wave infrared within coniferous forests, transmission is generally low making the assumption reasonable for most studies (Drake *et al.*, 1999; Roberts *et al.*, 1993).

The image processing software package ENVI<sup>®</sup> 3.6 (RSI, 2003) was used to undertake the unmixing analysis. A minimum noise fraction (MNF) technique was used to derive the spectra of pure cover types by transforming the spectral data into a reduced number of channels containing independent information thereby reducing noise in the data (Green *et al.*, 1988). These new MNF transformed bands were then analyzed to find the most "spectrally pure" (extreme) pixels in the image using a Pixel Purity Index (PPI) classifier (RSI, 2003). Clusters of extreme pixels in the image were then displayed and, through an iterative process which involved comparing the spectra with ground based reflectance spectra, examining the spatial mapping of endmembers, and comparing with local knowledge and field observations, a label was assigned to each "pure" cover class.

There are a number of components that contribute to the reflectance of an image scene including (a) basic scene objects such as soil and vegetation species, (b) their condition, and (c) their architecture or spatial arrangement. However, in reality, only a small number of endmembers are capable of accounting for the spectral variation. For example a study by Roberts *et al.* (1993) demonstrated that over 98 percent of the spectral variation in Airborne Visible/Infrared Imaging Spectrometer (AVIRIS) imagery was accounted for by a combination of three basic endmembers: green vegetation, shadow, and soil. Shadow has been found to be an important endmember and has been highly correlated with canopy structure (Peddle *et al.*, 1999), resulting in associated relationships with

other biophysical variables such as biomass, net primary productivity (NPP), and leaf area index (LAI) being expected. In stressed, defoliated crowns with reduced canopy biomass, the amount of shadow will vary as crowns transmit more radiation into the gaps. As a result the amount of between crown shadow as well as the brightness of the shadow may increase (Seed and King, 2003). Wood or non-photosynthetic vegetation (NPV) have also been shown to be valuable endmembers to include when analyzing forested scenes (Roberts *et al.*, 1993; Fitzgerald *et al.*, 2002). Levesque and King (2003) identified wood, shadow, mineral tailings, and vegetation as key endmembers that explained the variability in their multispectral imagery. In this study four endmembers were selected to characterize the variance in the imagery: sunlit canopy, soil, shadow, and non-photosynthetic vegetation. Once selected the image fractions were computed based on a constrained model with low average root mean square error (RMSE) (Fitzgerald *et al.*, 2002; Elmore *et al.*, 2000) and normalized (Dennison and Roberts, 2003; Souza *et al.*, 2003).

Field measurements of crown structure and condition were statistically compared to the spectral indices and the image fractions using the statistical package Statistica (Stat Soft, Ltd., 2002). Initially, correlations were determined between the raw spectral bands, the indices, and the endmember contributions to show degree of co-linearity between variables. Prior to developing multi-regression models for particular forest attributes, it is critical to ensure that there is not high co-linearity among predictor variables which may artificially inflate the variance accounted for. This may be the situation, for the endmember models as the four image endmember fractions must add up to 1.0 (i.e., as one endmember increases, others must decrease). As a result, correlation matrices for the mean endmember values within each crown were derived. A conscious decision was then made to bias the comparison between the spectral indices and the endmember analysis. Conventionally, most functional and/or empirical relationships derived using spectral indices only utilize a single index, rather than a more complex function which combines multiple indices. This is because the indices are assumed to infer a simple biophysical vegetation attribute. By comparison, when investigating relationships between vegetation attributes and fraction endmember datasets, it is more intuitive that the resulting relationship will be a function of a number of endmembers, for example sunlit crown and shadow, rather than simply a single index. As a result, simple linear regression and correlation analysis were used for the vegetation index analysis, and multiple linear regression was used for the endmember study. In order to account for the additional explanatory variables in the endmember analysis, the adjusted correlation coefficient value were used which takes into account the number of input variables. Forward stepwise regression techniques were used to assess the significance of each individual fraction image and build models with forest attributes. If the correlation coefficient between endmembers was high ( $r^2 > 0.8$ ), only the most significant endmember was allowed to enter the model with the other discarded from the analysis. When modeling the binary field attributes (presence of dead leader and presence of discoloration) a generalized linear modeling (GLM) approach using a logistic function was used which explicitly recognizes the presence/absence nature of the attribute.

## Results

### Spectral Indices

Figure 1 provides a 250 × 250 m subset of the CASI-2 imagery with canopies experiencing a range of *S. sapinea* infection.

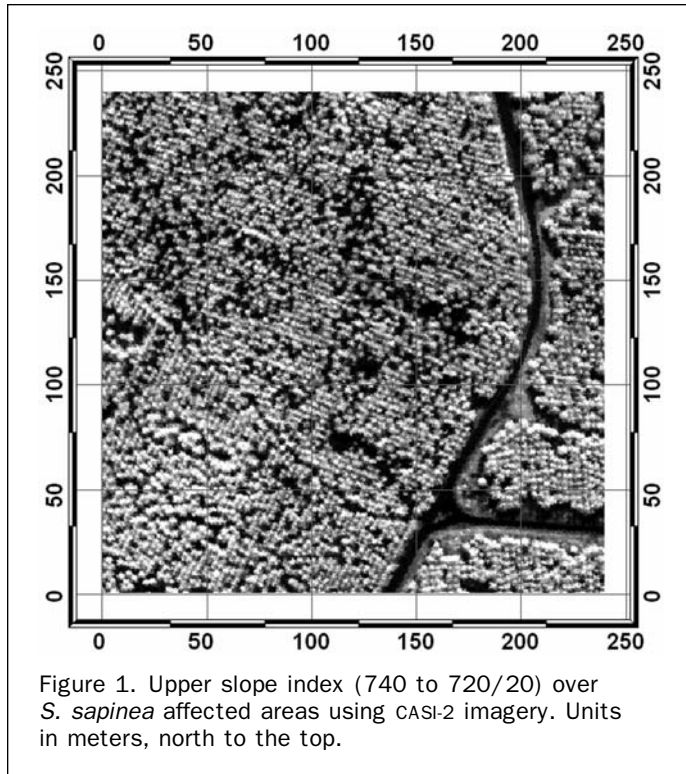


Figure 1. Upper slope index (740 to 720/20) over *S. sapinea* affected areas using CASI-2 imagery. Units in meters, north to the top.

The image displays a grayscale representation of the upper slope of the red-edge calculated between 710 to 740 nm. Brighter clusters indicate healthier crowns with dark areas indicating regions of soil and non-photosynthetically active vegetation. A road, for plantation access, is clearly visible along the western side of the image, and the patchwork nature of the plantation establishment can be seen with a general south west alignment. Crowns with both high and low levels of infection have been marked for clarity.

Using correlation and regression analysis, each of the individual crown attributes were compared to the mean crown spectral indices listed in Table 3. Of the 78 crowns identified on the imagery, four were flagged by field crews as possibly mismatched between the crown delineation on the imagery and the field scores and were subsequently removed from the analysis. Table 4 shows the overall ranking of the first three most-highly correlated reflectance indices, and the least correlated for crown leader color, color of the upper quartile, overall crown color, and stem DBH. In addition to their rank, the standard errors of the observation are shown. The table demonstrates the range of relationships between the spectral indices and the individual crown attributes with coefficients of determination ( $r^2$ ) ranging from very poor (0) to highly significant (0.70,  $p < 0.001$ ).

Investigating the color-based assessment of crown condition first, Figure 2 shows the relationship between the simple ratio of 710/690 nm ratio (Stone *et al.*, 2003) and the color of the crown leader (a six class variable where 1 is dark green, through light green, yellow, orange, red, and 6 is grey) obtained for *S. sapinea* affected crowns. As discussed previously, the presence of orange and red needles along the leader is often a first indication of the presence of *S. sapinea* crowns. Figure 2 shows a trend with higher index values (corresponding to an increase in chlorophyll absorption at 690 nm) being associated with a dark green leader color ( $r^2 = 0.70$ ,  $se = 0.99$  color units,  $p < 0.001$ ).

Correlation analysis of the crown attribute data confirm that there is a very high correlation between the top two quartiles of the crown ( $r^2 > 0.95$ ) indicating that both physiologically, and spectrally, there is little difference in crown condition from the top to the middle of the tree crown. As a result, it is possible to represent the quartile color crown information as a single crown quartile variable rather than analyze each quartile individually. Figure 3 shows the relationship with the most consistent linear trend between the CASI upper slope of the red-edge and crown color of the top quartile ( $r^2 = 0.65$ ,  $se = 1.02$  color units,  $p < 0.001$ ). Figure 4 shows relationship between the upper slope of the red-edge and the mean crown color which is also highly significant ( $r^2 = 0.70$ ,  $se = 0.17$  mean color units,  $p < 0.001$ ).

Overall, Table 4 indicates that the four spectral indices with the strongest relationships with the individual crown attributes were the modified normalized index of Sims and Gamon (2002), ( $mND_{index}$ ), the slope of the upper red-edge, the Carter (1994) index (R690/R750), and the 710/690 nm chlorophyll index of Stone *et al.* (2003).

Using the logistic modeling approach, a null model was fitted which describes the overall deviance within the two related variables. Once a logistic model is applied this null deviance is compared to the deviance which is explained by the logistic model. Attributes which explain the largest amounts of deviance (and are therefore highly statistically significant) correspond to the most highly correlated variable, as in normal regression analysis. Table 4 indicates that the deviance of the null model for presence of discoloration is 90.87 with the Carter (1994) C1 and C3 indices (see Table 3 for notation) explaining the most deviance when fitted with a logistic regression model. By contrast, the median of the red-edge explained the least deviance in the model.

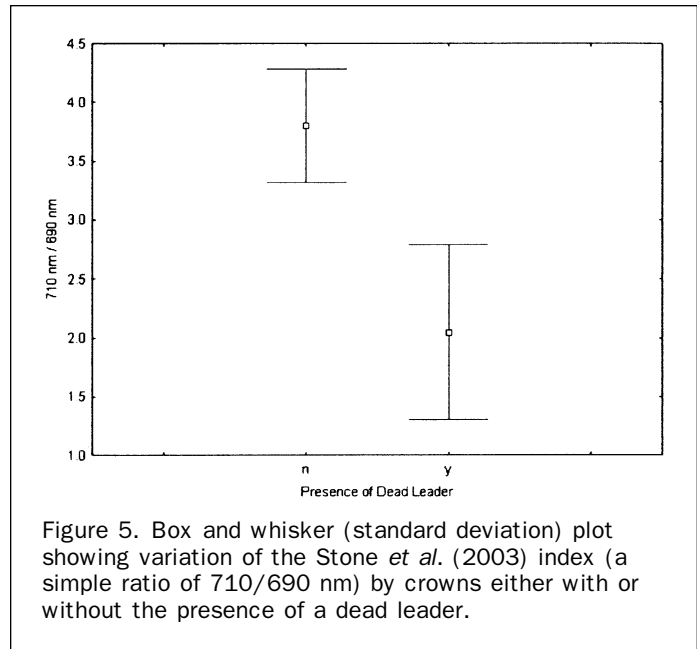
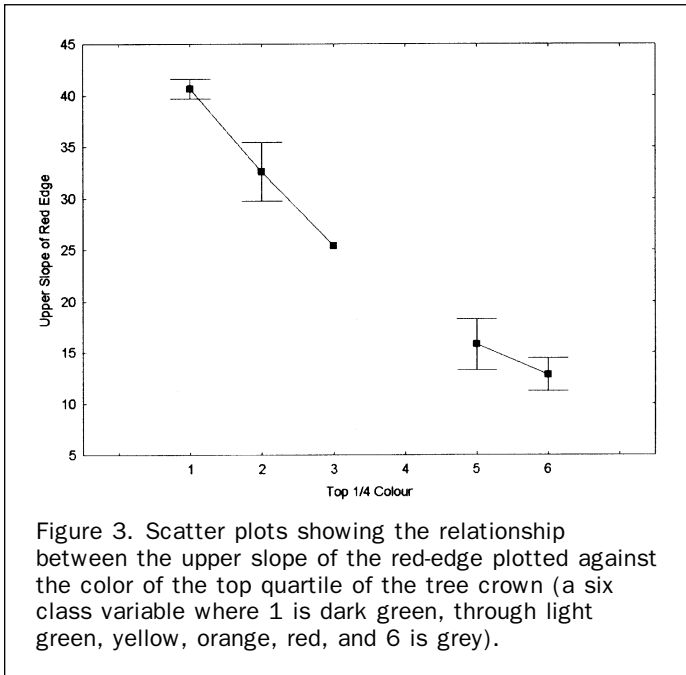
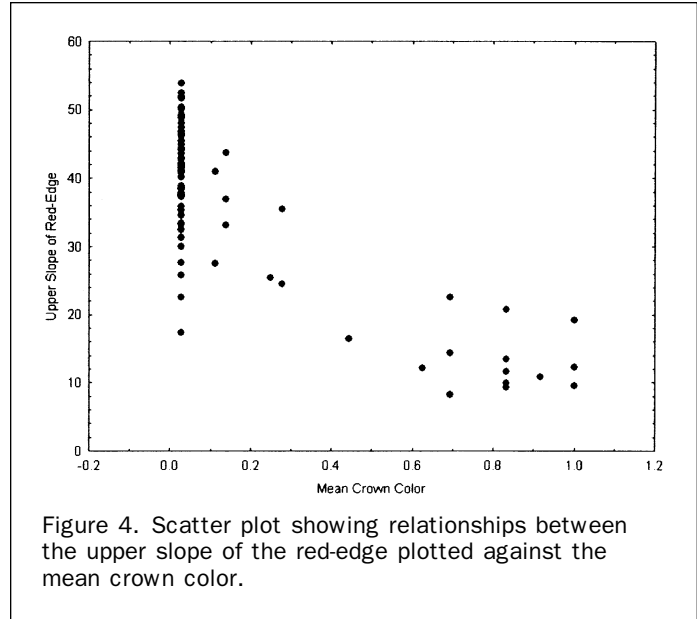
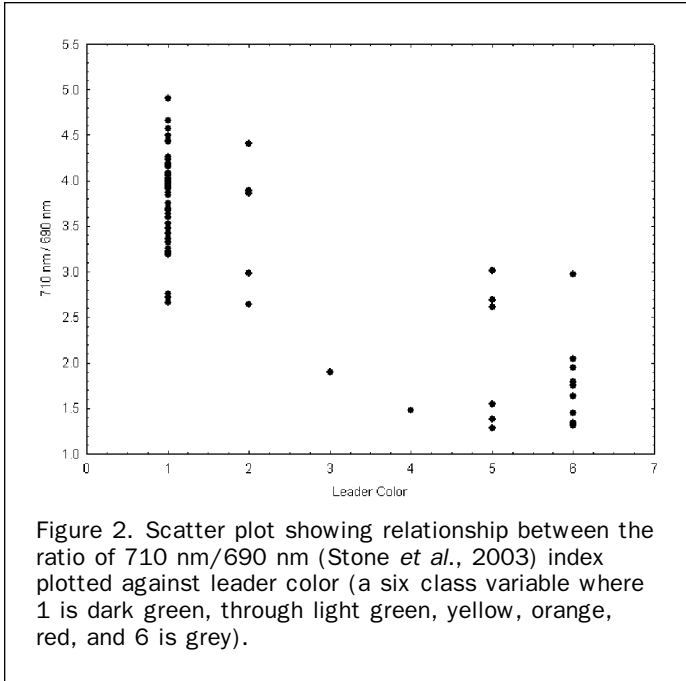
Figure 5 shows the relationship between the presence of the dead leader and the 710/690 nm ratio (Stone *et al.*, 2003). A diagnostic feature of *S. sapinea* infection in *P. radiata* trees, particularly in the later stages, is the presence of a dead leader, and as expected, the Figure confirms that crowns with a dead leader have lower values for the 710/690 nm ratio than the crowns with a live leader.

#### Spectral Mixture Analysis

Figure 6 illustrates the endmember spectral curves for both the UniSpec field-based spectra collected during the field

TABLE 4. TOP THREE CORRELATION COEFFICIENTS IN ADDITION TO LEAST SIGNIFICANT SPECTRAL INDEX AGAINST FIVE KEY FOREST ATTRIBUTES WITH *S. SAPINEA* INFECTED STANDS (N = 74) (SEE TABLE 3 FOR FULL INDEX NAMES AND DERIVATION)

	Leader Color	$r^2$	se	Top 1/4 Color	$r^2$	se	Mean Crown Color	$r^2$	se	Presence of Discoloration	Null Dev.	Exp. Dev.	DBH	$r^2$	se
Rank 1	Stone	0.70	0.99	$mND_{index}$	0.69	0.92	Upper RE	0.70	0.17	Carter (C3)	90.87	54.3	Mean RE	0.27	2.77
Rank 2	$mND_{index}$	0.66	1.05	Stone	0.69	0.93	$mND_{index}$	0.68	0.17	Carter (C1)	90.87	48.2	Median RE	0.27	2.78
Rank 3	Carter (C1)	0.64	1.09	Upper RE	0.69	0.95	Stone	0.68	0.18	PSRI	90.87	48.16	Max RE	0.15	3.00
Last	Median RE	0.13	1.71	Median RE	0.14	1.55	Median RE	0.18	0.27	Median RE	90.87	3.28	Carter (C1)	0.01	3.28



campaign and image based spectra computed from MNF and PPI analysis. In the case of the UniSpec spectra, which has a finer spectral resolution, the spectra over each CASI band width were averaged for the comparison. The two sets of spectra correspond closely indicating the endmembers identified on the image represent the actual endmembers well. While the shadow endmember spectra can not be reliably obtained in the field, it is apparent on the imagery as an endmember due to its near zero reflectance across the twelve spectral bands. Figure 6 also indicates there is good correspondence between the field spectra obtained for brown (non-photosynthetic) needles and the NPV endmem-

ber, as well as between spectra of soil and its respective endmember.

Figure 7 shows the four computed image fractions (sunlit crown, shadow, soil, and NPV) for one of the *S. sapinea* plots in the CASI-2 imagery. The image fraction images illustrate clear differentiation in abundances between the key endmembers. Individual tree crowns are identifiable on the sunlit crown fraction, with the shadow fraction providing an inverse image of the sunlit crowns. The fractions indicate that shadow is well distributed throughout the forest stands with the high shadow fractional values most evident along roads where the forest edge has been created. NPV has scattered patches of high fractional abundance where there are clusters of brown needles (within tree crowns and on the ground) and along the roadside (possibly a misclassification with soil). The soil fractional endmember shows localized areas of high abundance primarily along the

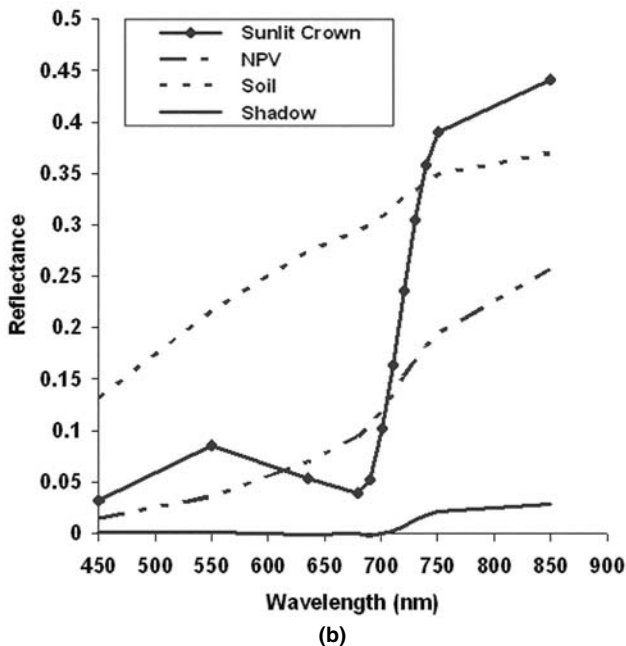
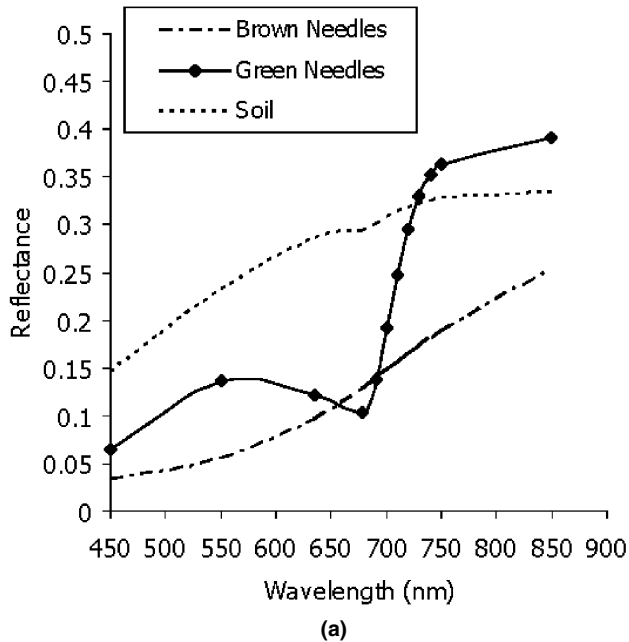


Figure 6. Spectral curves for endmembers derived from (a) CASI-2 Imagery and (b) field spectra.

roads where a considerable amount area of soil has been exposed.

Figure 8 displays the relationships between the four endmember (sunlit crown, shadow, NPV, and soil image fractions) and leader color for *S. sapinea* affected crowns. Strong relationships exist for the sunlit crown and NPV image fractions with  $r^2$  values of 0.62 ( $p < 0.001$ ) and 0.71 ( $p < 0.001$ ), respectively, derived predominantly by crowns at either end of the color scale. The sunlit crown fractional abundance decreases with a change in color from dark green to grey with opposite trends for NPV fractional abundance.

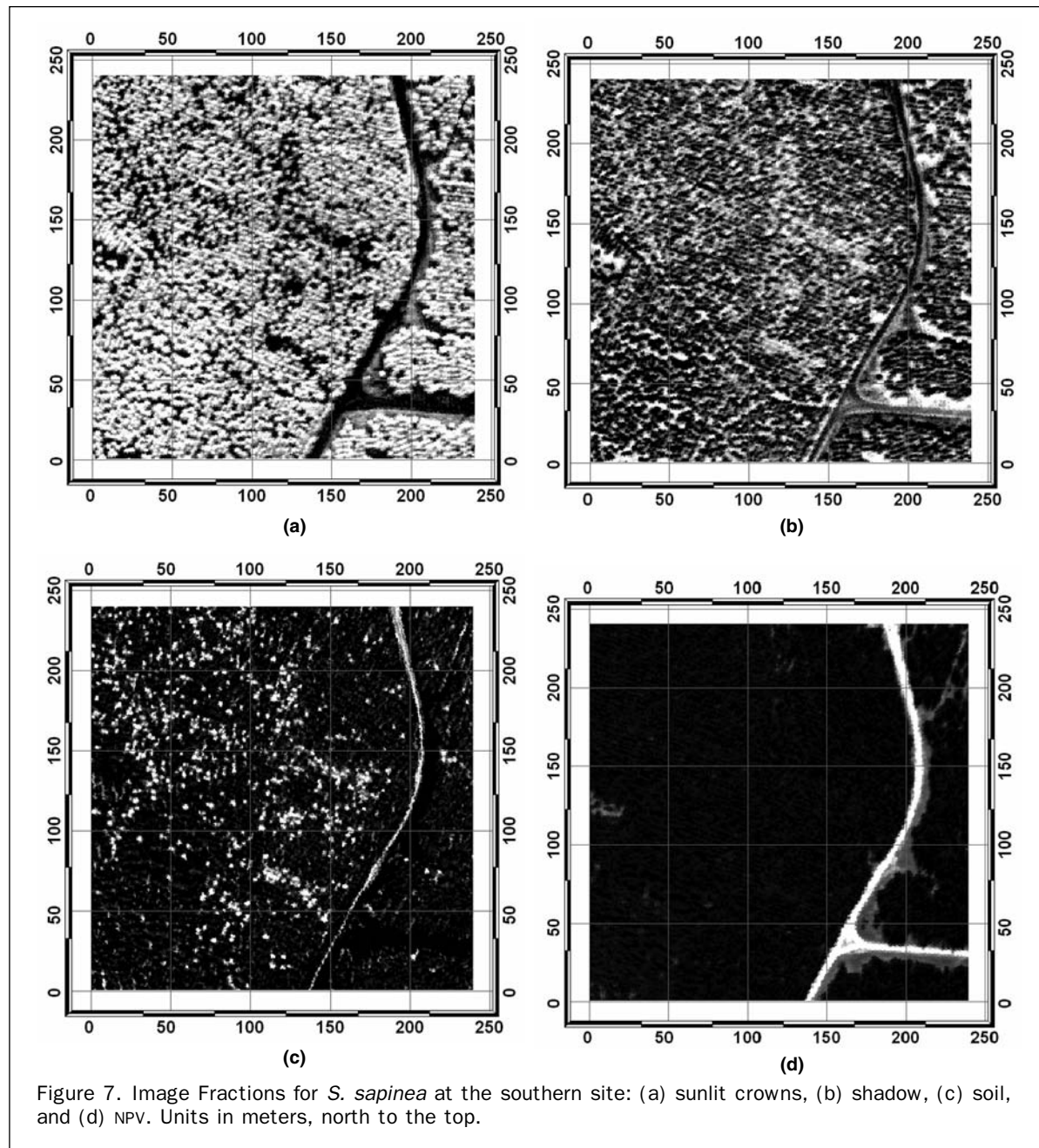
A slightly weaker relationship is indicated for the shadow image fraction ( $r^2 = 0.40$ ,  $p < 0.00$ ), with increasing fractional abundance values occurring as the leader color changes from dark green to grey. This increasing trend in the shadow fraction implies that needle loss, reduced crown size, and density all are having an effect on the shadow proportion. There is no clear relationship between leader color and fractional abundance of soil ( $p > 0.05$ ). The relationship between *S. sapinea* mean crown color attribute was also strong (not shown) with the four image fractions. Again NPV is the most highly correlated ( $r^2 = 0.7$ ,  $p < 0.001$ ) as is the sunlit crown endmember ( $r^2 = 0.56$ ,  $p < 0.001$ ). The shadow endmember is slightly weaker with a positive relationship with overall crown color. Similar to results of the health attribute leader color, the soil endmember has no clear relationship with overall crown color. Table 5 provides a summary of the individual correlations (and the explained deviance for the presence of discoloration), and indicates that the soil fraction is the only endmember to not have a highly significant relationship ( $p < 0.001$ ) with any crown attribute.

Table 6 shows the results of the multiple stepwise regression for each of the *S. sapinea* crown attributes. Using a stepwise regression approach, for both the normal and logistic regression allows the most significant (based on pre-defined  $f$ -enter and  $f$ -exit values) image fractions to be selected. The models for leader color and mean crown color are similar with both being highly significant (adjusted  $r^2$  of 0.73 and 0.67, respectively; for both  $p < 0.001$ ). In both cases, either one or two additional outliers were removed from the analysis. The most significant fraction selected by the regression is NPV followed by the shadow fractions. While sunlit canopy was not significantly correlated with NPV it is clear that, of the endmembers, they are the most highly linked, and as a result, do not both enter the final model. The models produce a standard error, in the case of leader color less than one color unit, and in the case of the mean crown color, around 15 percent. In the case of presence of discoloration the Generalized Linear Model (GLM) model selects only the sunlit fraction as the most significant variable in the model with the remaining three being insignificant for model prediction.

Figure 9 shows the relationship between the presence of the dead leader and the four image fractions. The diagnostic feature of the dead leader with *S. sapinea* infection is important when trying to understanding the spectral response of the crown cluster. The Figure confirms that when there is no dead leader (i.e., the crown has little or no *S. sapinea* infection) the proportion of the tree crowns with soil and NPV fractions is very low, typically less than 8 percent of the total crown. By comparison the shadow fraction is around 20 percent with the sunlit crown as the most dominant at 80 percent. In crowns which have a dead leader (i.e., the crown has high *S. sapinea* infection), the soil fraction remains the same while the sunlit crown proportions have fallen significantly to 25 percent, and the shadow and NPV components have increased. The relationship between the sunlit crown and NPV image fractions (not shown) is strongly negative ( $r^2 = 0.59$ ) indicating, as expected, that the fraction of sunlit crown increases while the proportion of NPV decreases. These two results combined indicate that a method to assess for the presence or absence of a dead leader may be possible, simply by taking the ratio of the sunlit crown fraction and the NPV fraction.

## Discussion

Spectral indices in controlled laboratory and operational environments have been demonstrated to be successful at



assessing vegetation condition with respect to chlorophyll content and function (Datt, 1998; Zarco-Tejada *et al.*, 2002). A number of these studies have also replicated strong relationships at the canopy scale using remotely sensed imagery obtained from hyperspectral sensors (Coops *et al.*, 2002); however, problems can arise at this scale preventing accurate assessment of vegetation condition. An issue of particular concern for spectral vegetation indices is when vegetation is stressed and has reduced chlorophyll pigment concentrations. This coupled with reduced overall overstorey vegetation cover and between crown openness makes the translation of regression-based responses from needle to crowns in stressed and open canopies more difficult.

In this study, a variety of standard and new vegetation indices have been assessed, and a number of significant relationships identified. The most significant indices relate

the chlorophyll absorption wavelengths from 680 to 700 nm with wavelengths in the near infrared region of the spectrum (such as 710 or 750 nm) or the slope of the upper red-edge between 710 and 740 nm. The selection of chlorophyll sensitive wavelengths is an important one. The main chlorophyll absorption feature lies approximately at 675 nm but becomes saturated at medium to high chlorophyll concentrations, and hence, wavelengths near 675 nm are more suitable for estimating low levels of chlorophyll (Carter and Knapp, 2001). It is believed that a common effect of *S. sapinea* infection in *P. radiata* stands is disruption of the translocation system in branches and the stem (A. Carnegie, SFNSW, personal communication). This would be expected to cause a decrease in stomatal conductance resulting in reduced photosynthesis, and then, upon depletion of the needle carbohydrate reserves, chlorophyll degradation

(chlorosis) and tissue dehydration, and ultimately disintegration of the needle structure (necrosis). Therefore, there is a progression of symptoms as the disease establishes itself, both at the needle scale and crown scale. The spectral wavelengths selected for inclusion into a generic index

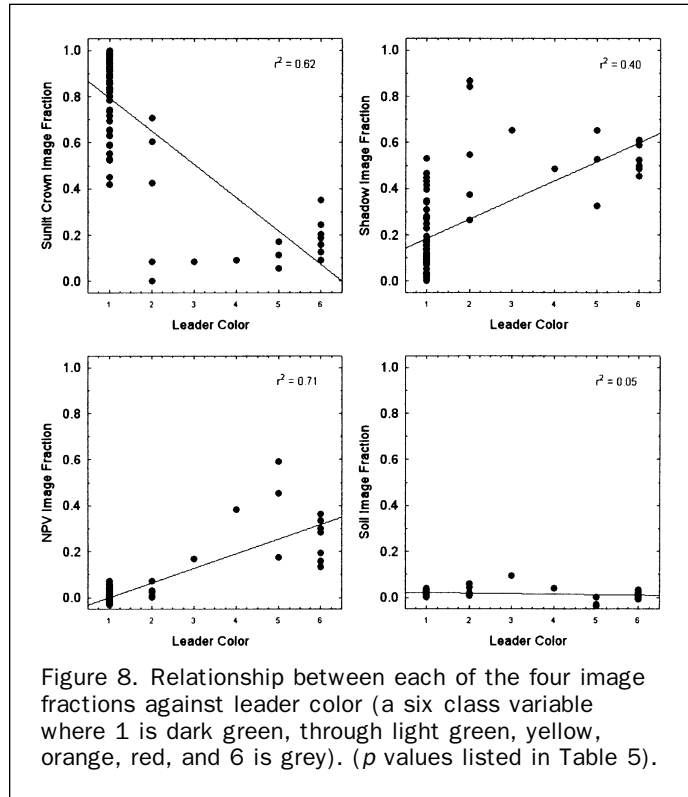


Figure 8. Relationship between each of the four image fractions against leader color (a six class variable where 1 is dark green, through light green, yellow, orange, red, and 6 is grey). ( $p$  values listed in Table 5).

TABLE 5. CORRELATIONS BETWEEN FIELD VARIABLES AND IMAGE FRACTIONS

Attribute	Sunlit Crown	Shadow	NPV	Soil	Null Deviance
Leader Color	0.62***	0.40***	0.71***	0.05	
Mean Crown Condition	0.56***	0.34***	0.70***	0.09*	
Top 1/4 Color	0.63***	0.40***	0.75***	0.06*	
Presence of Discoloration	69.4***	61.2***	49.4***	0.3	90.9

Note:  $\alpha < 0.05^*$ ,  $\alpha < .001^{**}$ ,  $\alpha < .0001^{***}$ .

TABLE 6. MULTIPLE LINEAR REGRESSION MODELS DEVELOPED FOR CROWN ATTRIBUTES AND FRACTIONAL ENDMEMBERS

Health Attribute	Image Fraction (In Order)	Level of Significance	$r^2$ Change	Standard Error of Estimate	No of Obs. (Outliers > 2*Sigma Removed)	Adjusted $r^2$
Leader Color	NPV	<.001	0.67	0.84	72	0.73
	Shadow	.001	0.06			
Mean Crown Color	NPV	<.001	0.63	0.14	73	0.67
	Shadow	.016	0.04			
DBH	NPV	<.001	0.19	2.38 (cm)	74	0.26
	Sunlit Crown	<.001	0.04			
	Soil	<.001	0.03			
Health Attribute	Image Fraction	Null-Deviance	Deviance Explained	No. of Observations		
Proportion of Discoloration	Sunlit Crown	90.0	69.4	74		

capable of categorizing both the extent and severity of *S.sapinea* symptoms in *P. radiata* canopies need to be sensitive to both the symptoms of chlorosis and necrosis. In most cases, field-based assessment of *S. sapinea* relies on a redness in the needle or a dead leader, which are both more readily associated with necrotic rather than chlorotic behavior; however, the detailed ground survey information obtained for this study and the significant correlation with chlorophyll-based indices (Stone *et al.*, 2003), and Carter (1994) indicates that chlorotic behavior, as well as necrotic (upper red-edge) trends, are being detected. The most highly correlated indices in this study (the modified normalized index of Sims and Gamon (2002), (mND<sub>index</sub>), the Carter (1994) index (R690/R750), and the recent 710/690 nm chlorophyll index of Stone *et al.* 2003) are all sensitive to chlorophyll content, and the upper red-edge index is sensitive to cellular structure. As the foliar symptoms of chlorosis and necrosis are confounded in most plant pathogens (e.g., Ayres 1992), a classification system of damage severity, which takes into account both these symptoms (chlorosis and necrosis), is desirable.

Both the spectral indices and the endmember fractions models suffer from a lack of observations in the mid-range of infection, and as a result the yellow and orange samples had only a small number of samples. It is important therefore to note, that some of the relationships are based on key trends between the healthy and dead tree samples, and that additional sampling is required in the middle range of damage to make fully robust models.

When selecting endmembers for the linear spectral unmixing the number is limited to one less than the total number of input bands (Smith *et al.*, 1994). In this case, seven minimum noise fraction images were extracted from the raw CASI-2 imagery which resulted in a maximum of six allowable endmembers to be defined. In this analysis, four endmembers were extracted from the imagery. Attempts to derive a fifth endmember which represented a grass and weed category, which was clearly visible alongside road side verges and compartment boundaries, proved difficult. This is principally due to the similar spectral response of the weed and grass endmember with several *P. radiata* crowns presumably with healthy new shoots. This highlights a limitation of the unmixing approach, as it does not account for spectral variation present within the same endmember (i.e., endmembers are assumed to be completely pure), with only a single endmember per material. Subsequently, unmixing endmembers representing different vegetation types is a difficult task that is compounded by spectral variability even within a single plant. In this study the endmember analysis was limited to the four endmembers with only one green vegetation endmember. This is a recognized issue when applying spectral unmixing on

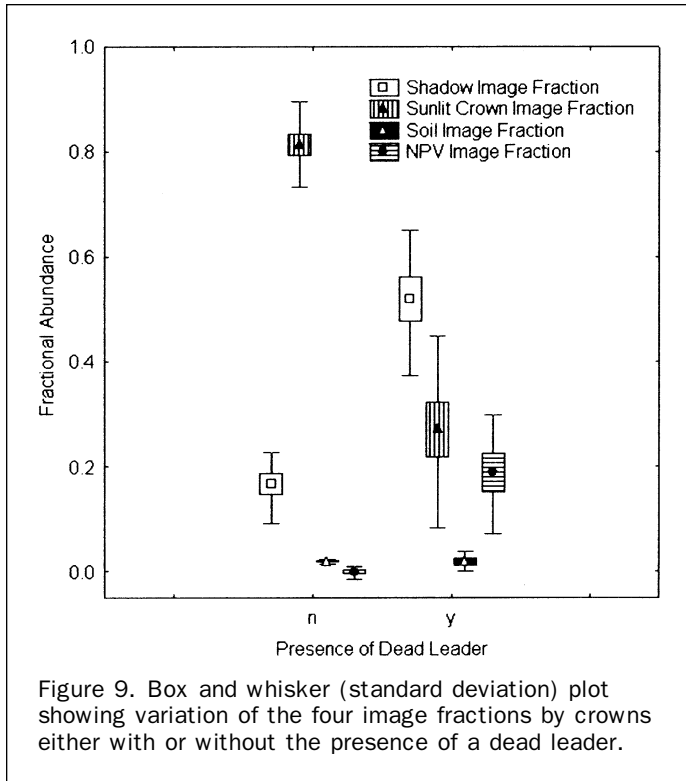


Figure 9. Box and whisker (standard deviation) plot showing variation of the four image fractions by crowns either with or without the presence of a dead leader.

datasets with small numbers of spectral wavelengths. Roberts *et al.* (1998) for example has developed a multiple endmember spectral mixture analysis (MESMA) which allows the number and type of endmembers to vary on a per pixel basis rather than using a fixed number of endmembers. Likewise, Bateson *et al.* (2000) developed the use of endmember bundles in spectral unmixing whereby a range of endmember abundance (maximum and minimum abundance images) is produced, rather than a fixed abundance value for each endmember.

An important outcome of the modeling process is the lack of the sunlit canopy fraction as a significant variable in explaining variation in three of the four individual crown health and condition attributes. Models for leader color, overall crown color and color of the top quarter of the crown (not shown) all utilize the NPV and the shadow fractions in their predictions, producing models of similar significance and explanatory power. The inclusion of an endmember for NPV appears important in the model results due principally to the higher proportion of dead or dying vegetation present in the scene from damaged trees and crowns. In previous studies the fractional abundance of NPV has had mixed levels of success due to misclassification with soil (Roberts *et al.*, 1993; Drake *et al.*, 1999; Okin and Roberts, 2000). This was not the case in this study, possibly due to generally low levels of exposed soil and the larger number of spectral bands in the visible and near infrared regions of the spectrum which allow the soil spectra to be clearly differentiated; a point also noted by Roberts *et al.* (1993). Part of the reason that the sunlit crown fraction was not selected in three of the models may be due to the relatively strong linear relationship between the sunlit canopy fraction and the NPV fraction (refer to Figure 8). It is probable that the information contained in the NPV fractional abundances can account for the forest condition variability contained within sunlit crown fractions.

The inclusion of a shadow endmember has been noted by Peddle *et al.* (1999) to be the most important forest component for predicting boreal forest biophysical variables and an under-utilized source of remote sensing information by Asner and Warner (2003). In the models produced by this study, the results have repeated these strong findings for shadow fraction. In a healthy forest, it is likely trees will grow and attempt to harness as much light as possible for photosynthetic activity forming dense individual crowns. This will in effect limit the amount of intra-crown shadowing. Unhealthy trees, in comparison, will experience thinning of the crowns, loss of branches and possibly stunted growth, as well as the formation of canopy gaps as trees begin to die. This will lead to higher shadowing both between and within unhealthy tree crowns.

Comparing the indices and unmixing models, the results indicate that spectral mixture analysis can provide similar predictions of forest biophysical and structural information to more conventional spectral vegetation indices derived from an airborne remote sensing imagery; although, it is recognized that the models developed using image fractions allowed more than one explanatory variable. DBH is poorly predicted from both the indices and the image fraction approach which is similar to other studies (Peddle *et al.*, 2001), and implies that more sophisticated analytical or modeling strategies are required. While different indices appear to be better suited to different forest health attributes, a clear benefit of the use of image fractions is the fact that the same variables (shadow and NPV fractions) were consistently used in all models making variable selection an easier process, as recommended from previous studies (i.e., Peddle *et al.*, (1999) and Roberts *et al.*, (1993)).

From results of this and other similar studies (Goodwin *et al.*, 2005), it is apparent that the use of image fractions and linear spectral unmixing analysis appears to represent a suitable approach for predicting crown condition information compared to spectral vegetation indices. The main success of the technique may lie in the ability of spectral mixture analysis to explicitly and directly detect the influence of background and shadows on overall pixel reflectance, an important aspect of stressed crowns, while vegetation indices do not. Despite all available vegetation spectral indices not being tested in this study, the ones tested cover a large range of indices including simple and normalized ratios, as well as red-edge slope indicators.

## Acknowledgments

This study is part of a research program applying remotely-sensed multispectral imagery to the classification of canopy damage from a range of damaging agents in *P. radiata* plantations supported by CSIRO Forestry and Forest Products, State Forests of NSW and by Forestry and Wood Products Research and Development Corporation, Melbourne as part of its PTR initiative. The project relied strongly on members of the State Forest of New South Wales (SFNSW) Forest Health Survey Unit (FHSU) led by Angus Carnegie, with Grahame Price, and Ian Hides (SFNSW). Michael Stanford, Ken Old, Mark Dudinski (CSIRO FFP) and Angus Carnegie (SFNSW) jointly developed the field assessment techniques used in this study, for which we are very grateful. Components of image processing and model developed were also undertaken by Michael Stanford (CSIRO FFP). We thank SFNSW for access to the relevant *P. radiata* plantations in NSW to undertake the field work, and Dr. Laurie Chisholm (University of Wollongong) for collecting ground based spectra. Anders Siggins and Dr. Bisun Datt (CSIRO) provided useful comments on drafts of the manuscript.

## References

- Asner, G.P., and A.S. Warner, 2003. Canopy shadow in IKONOS satellite observations of tropical forests and savannas, *Remote Sensing of Environment*, 87:521–533.
- Ayres, P.G., 1992. *Pests and Pathogens: Plant Responses to Foliar Attack*, Environmental Plant Biology Series, Scientific Publishers, Oxford, UK.
- Bateson, C.A., G.P. Asner, and C.A. Wessman, 2000. Endmember bundles: A new approach to incorporating endmember variability into spectral mixture analysis, *IEEE Transactions on Geoscience and Remote Sensing*, 38:1083–1094.
- Bollman, M.P., G.B. Sweet, D.A. Rook, and E.A. Halligen, 1986. The influence of temperature, nutrient status and short drought on seasonal variation of primordia and shoot elongation in *Pinus radiata*, *Canadian Journal of Forest Research*, 16:1019–1029.
- Carter, G.A., 1994. Ratios of leaf reflectances in narrow wavebands as indicators of plant stress, *International Journal of Remote Sensing*, 15:697–703.
- Carter, G.A., and A.K. Knapp, 2001. Leaf optical properties in higher plants: Linking spectral characteristics to stress and chlorophyll concentration, *American Journal of Botany*, 88: 677–684.
- Carter, G.A., and R.L. Miller, 1994. Early detection of plant stress by digital imaging within narrow stress-sensitive wavebands, *Remote Sensing of Environment*, 50:295–302.
- Coops, N.C., C. Stone, D.S. Culvenor, L. Chisholm, and R. Merton, 2002. Predicting chlorophyll content in Eucalypt vegetation at the leaf and canopy level using high spectral resolution imagery, *Tree Physiology*, 23:23–31.
- Datt, B., 1998. Remote sensing of chlorophyll a, chlorophyll b, chlorophyll a + b, and total carotenoid content in Eucalyptus leaves, *Remote Sensing of Environment*, 66:111–121.
- Datt, B., 1999. A new reflectance index for remote sensing of chlorophyll content in higher plants: Tests using Eucalyptus leaves, *Journal of Plant Physiology*, 154:30–36.
- Dennison, P.E., and D.A. Roberts, 2003. The effects of vegetation phenology on endmember selection and species mapping in southern California chaparral, *Remote Sensing of Environment*, 87:295–309.
- Drake, N.A., S. Mackin, and J.J. Settle, 1999. Mapping vegetation, soil, and geology in semiarid shrublands using spectral matching and mixture modelling of SWIR AVIRIS imagery, *Remote Sensing of Environment*, 68:12–25.
- Elmore, A.J., J.F. Mustard, S.J. Manning, and D.B. Lobell, 2000. Quantifying vegetation change in semiarid environments: Precision and accuracy of spectral mixture analysis and the normalised difference vegetation index, *Remote Sensing of Environment*, 73:87–102.
- Farrand, W.H., R.B. Singer, and E. Merenyi, 1993. Retrieval of apparent surface reflectance from AVIRIS data: A comparison of empirical line, radiative transfer and spectral mixture methods, *Remote Sensing of Environment*, 47:311–321.
- Fitzgerald, G.J., S.J. Maas, and W.R. DeTar, 2002. Detecting spider mite damage in cotton through spectral mixture analysis of AVIRIS imagery, *Proceedings of the 11<sup>th</sup> Airborne Visible/Infrared Imaging Spectrometer (AVIRIS) Workshop*, Jet Propulsion Laboratory, Pasadena, California.
- Franklin, S.E., 2000. *Remote Sensing for Sustainable Forest Management*, Lewis Publishers, London.
- Garcia-Haro, F.J., M.A. Gilabert, and J. Melia, 1999. Extraction of endmembers from spectral mixtures, *Remote Sensing of Environment*, 68:237–253.
- Gausman, H.W., 1985. *Plant Leaf Optical Properties in Visible and Near-infrared Light*, Graduate Thesis, Texas Tech University (No. 29), Texas Technical Press, Lubbock, Texas, p. 78.
- Gitelson, A.A., U. Gritz, and M.N. Merzlyak, 2003. Relationships between leaf chlorophyll content and spectral reflectance and algorithms for non-destructive chlorophyll assessment in higher plant leaves, *Journal of Plant Physiology*, 160:271–282.
- Gitelson, A.A., and M.N. Merzlyak, 1996. Signature analysis of leaf reflectance spectra: Algorithm development for remote sensing of chlorophyll, *Journal of Plant Physiology*, 148:495–500.
- Goodwin, N., N.C. Coops, and C. Stone, 2005. Quantifying forest canopy condition from airborne imagery using spectral mixture analysis and fractional abundances, *International Journal of Applied Earth Observation and Geoinformation*, 7:11–28.
- Gougeon, F.A., 1999. Automated individual tree crown delineation using a valley-following algorithm and rule-based system (D.A. Hill and D.G. Leckie, editors), *Proceedings of the International Forum: Automated Interpretation of High Spatial Resolution Digital Imagery for Forestry*, 10–12 February, Victoria, B.C., Canada.
- Green, A.A., M. Berman, P. Switzer, and M.D. Graig, 1988. A transformation for ordering multispectral data in terms of image quality with implications for noise removal, *IEEE Transactions on Geoscience and Remote Sensing*, 26:65–74.
- Huete, A.R., 1988. A soil adjusted vegetation index (SAVI), *Remote Sensing of Environment*, 25:295–309.
- Li, X., and A.H. Strahler, 1985. Geometric-optical modelling of a conifer forest canopy, *IEEE Transactions on Geoscience and Remote Sensing*, GE-23:705–721.
- Leckie, D.G., X. Yuan, D.P. Ostaff, H. Piene, and D.A. Maclean, 1992. Analysis of high resolution multispectral MEIS imagery for spruce budworm damage assessment on a single tree basis, *Remote Sensing of Environment*, 40:125–136.
- Lewis, N.B., and I.S. Ferguson, 1993. *Management of Radiata Pine*, Inkata Press, Melbourne.
- Levesque, J., and D. King, 1999. Airborne digital camera image semivariance for evaluation of forest structural damage at an acid mine site, *Remote Sensing of Environment*, 68:112–124.
- Levesque, J., and D.J. King, 2003. Spatial analysis of radiometric fractions from high-resolution multispectral imagery for modelling individual tree crown and forest canopy structure and health, *Remote Sensing of Environment*, 84:589–602.
- Merton, R.N., 1999. *Multi-Temporal Analysis Of Community Scale Vegetation Stress With Imaging Spectroscopy*, Ph.D. Thesis, Department of Geography, University of Auckland, New Zealand.
- Merzlyak, M.N., A.A. Gitelson, O.B. Chikunova, and V.Y. Rakitin, 1999. Non-destructive optical detection of pigment changes during leaf senescence and fruit ripening, *Physiologia Plantarum*, 106:135–141.
- Okin, G.S., and D.A. Roberts, 2000. Linear unmixing of simulated, noisy spectra: Vegetation detection limits in areas of low cover, *Proceedings of the 9<sup>th</sup> Airborne Visible/Infrared Imaging Spectrometer (AVIRIS) Workshop*, Jet Propulsion Laboratory, Pasadena, California.
- Olthof, I., and D.J. King, 2000. Development of a forest health index using multispectral airborne digital camera imagery, *Canadian Journal of Remote Sensing*, 26:166–176.
- Peddle, D.R., F.G. Hall, and E.F. LeDrew, 1999. Spectral mixture analysis and geometric-optical reflectance modelling of boreal forest biophysical structure, *Remote Sensing of Environment*, 67:288–297.
- Peddle, D.R., S.P. Brunke, and F.G. Hall, 2001. A comparison of spectral mixture analysis and ten vegetation indices for estimating Boreal forest biophysical information from airborne data, *Canadian Journal of Remote Sensing*, 27(6):627–635.
- Peñuelas, J., I. Filella, P. Lloret, F. Munoz, and M. Vilajeliu, 1995. Reflectance assessment of plant mite attack on apple trees, *International Journal of Remote Sensing*, 16:2727–2733.
- Peñuelas, J., J. Pinol, R. Ogaya, and I. Filella, 1997. Estimation of plant water concentration by the reflectance water index (WI, R900/R970), *International Journal of Remote Sensing*, 18:2869–2875.
- Roberts, D.A., M. Gardner, R. Church, S. Ustin, G. Scheer, and R.O. Green, 1998. Mapping chaparral in the Santa Monica Mountains using multiple endmember spectral mixture models, *Remote Sensing of Environment*, 65:267–279.
- Roberts, D.A., M.O. Smith, and J.B. Adams, 1993. Green vegetation, nonphotosynthetic vegetation, and soils in AVIRIS data, *Remote Sensing of Environment*, 44:255–269.
- Research Systems Institute (RSI), 2003. *ENVI Image Analysis Systems*, Boulder Colorado.
- Seed, E.D., and D.J. King, 2003. Shadow brightness and shadow fraction relations with effective LAI: Importance of canopy

- closure and view angle in mixedwood boreal forest, *Canadian Journal of Remote Sensing*, 29(3):324–335.
- Shepherd, P.R., J.R. Freemantle, S. McArdle, and J.R. Miller, 1995. A comparison of different operational reflectance generation methods applied to airborne CASI imagery, *Proceedings of the 17th Canadian Symposium on Remote Sensing*, Saskatoon, Saskatchewan, Volume 1, pp. 268–273.
- Sims, D.A., and J.A. Gamon, 2002. Relationships between leaf pigment content and spectral reflectance across a wide range of species, leaf structures and development stages, *Remote Sensing of Environment*, 81:337–354.
- Smith, M.O., I.B. Adams, and D.E. Sabol, 1994. Spectral mixture analysis-new strategies for the analysis of multi spectral data, *Imaging Spectrometry – A Tool for Environment Observations* (I. Hill and I. Megier, editors), The Netherlands, Kluwer Academic Publishers, Boston, Massachusetts, pp. 125–144.
- Souza, C. Jr., L. Firestone, L.M. Silva, and D.A. Robert, 2003. Mapping forest degradation in the eastern Amazon from SPOT 4 through spectral mixture models, *Remote Sensing of Environment*, 87:494–506.
- Spanner, M.A., L.L. Pierce, D.L. Peterson, and S.W. Running, 1990a. Remote sensing of temperate coniferous forest leaf area index: The influence of canopy closure, understorey vegetation and background reflectance, *International Journal of Remote Sensing*, 11:95–111.
- Spanner, M.A., L.L. Pierce, S.W. Running, and D.L. Peterson, 1990b. The seasonality of AVHRR data of temperate coniferous forests: Relationships with leaf area index, *Remote Sensing of Environment*, 33:97–112.
- StatSoft, Ltd., 2002. Statistica (Data Analysis Software System), Version 6.2.
- Stone, C., L. Chisholm, and S. McDonald, 2003. Spectral reflectance characteristics of *Pinus radiata* needles infected with *Dothistroma* needle blight, *Canadian Journal of Botany*, 81:560–569.
- Treitz, P., and P. Howarth, 1996. *Remote Sensing Forest Ecosystem Characterization: A Review*, NODA/NFP Technical Report TR-12, Natural Resources Canada and Canadian Forest Service, Ontario, Canada.
- Thenkabail, P.S., R.B. Smith, and E. De Pauw, 2000. Hyperspectral vegetation indices and their relationships with agricultural crop characteristics, *Remote Sensing of Environment*, 71:158–182.
- Ustin, S.L., Q.J. Hart, L. Duan, and G.J. Scheer, 1995. Vegetation mapping on hardwood rangelands in California, *International Journal of Remote Sensing*, 17:3015–3036.
- Van Der Meer, F., and S.M. De Jong, 2000. Improving the results of spectral unmixing of Landsat Thematic Mapper imagery by enhancing the orthogonality of end-members, *International Journal of Remote Sensing*, 21:2781–2797.
- Will, G., 1985. *Nutrient Deficiencies and Fertiliser Use in New Zealand Exotic Forests*, FRI Bulletin No. 97, Forest Research Institute, New Zealand Forest Service, Rotorua, New Zealand.
- Wulder, M., R. Hall, N.C. Coops, and S. Franklin, 2004. High spatial resolution remotely-sensed data for the study of forest ecosystems, *BioScience*, 54:511–521.
- Zarco-Tejada, P.J., J.R. Miller, G.H. Mohammed, T.L. Noland, and P.H. Sampson, 2002. Vegetation stress detection through Chlorophyll a + b estimation and fluorescence effects on hyperspectral imagery, *Journal of Environmental Quality*, 31:1433–1441.

(Received 27 October 2004; accepted 17 March 2005; revised 21 April 2005)